AGU PUBLICATIONS

Geophysical Research Letters

RESEARCH LETTER
10.1002/2016GL069868

Key Points:
- The self-secondary crater population formed by Hokusai is unambiguously recognized
- Impact spallation forms self-secondaries, and they are inherent to all planetary complex craters
- Dominance of self-secondaries on crater materials varies with both location and age

Supporting Information:
- Supporting Information S1
- Table S1

Correspondence to:
Z. Xiao,
zyxiao@cug.edu.cn

Citation:
Xiao, Z., N. C. Prieur, and S. C. Werner (2016), The self-secondary crater population of the Hokusai crater on Mercury, *Geophys. Res. Lett.*, *43*, 7424–7432, doi:10.1002/2016GL069868.

Received 3 JUN 2016
Accepted 7 JUL 2016
Accepted article online 12 JUL 2016
Published online 30 JUL 2016

The self-secondary crater population of the Hokusai crater on Mercury

Zhiyong Xiao[1,2,3], Nils C. Prieur[3], and Stephanie C. Werner[3]

[1]Planetary Science Institute, School of Earth Sciences, China University of Geosciences, Wuhan, China, [2]Space Science Institute, Macau University of Science and Technology, Macau, China, [3]Centre for Earth Evolution and Dynamics, University of Oslo, Oslo, Norway

Abstract Whether or not self-secondaries dominate small crater populations on continuous ejecta deposits and floors of fresh impact craters has long been a controversy. This issue potentially affects the age determination technique using crater statistics. Here the self-secondary crater population on the continuous ejecta deposits of the Hokusai crater on Mercury is unambiguously recognized. Superposition relationships show that this population was emplaced after both the ballistic sedimentation of excavation flows and the subsequent veneering of impact melt, but it predated the settlement and solidification of melt pools on the crater floor. Fragments that formed self-secondaries were launched via impact spallation with large angles. Complex craters on the Moon, Mercury, and Mars probably all have formed self-secondaries populations. Dating young craters using crater statistics on their continuous ejecta deposits can be misleading. Impact melt pools are less affected by self-secondaries. Overprint by subsequent crater populations with time reduces the predominance of self-secondaries.

1. Introduction

When the Surveyor 7 mission was landed on the continuous ejecta deposits of the lunar Tycho crater, *Shoemaker et al.* [1969] noticed that close to the landing site, surfaces with different textures had up to 10 times different crater densities. Together with the melt flows and ponds observed nearby, the self-secondary cratering hypothesis was introduced to explain the crater density variation [*Shoemaker et al.*, 1969], i.e., self-secondaries are formed by near-vertically launched ejecta that have larger trajectory times than ejecta that formed the continuous ejecta deposit. This hypothesis is critical to the understanding of impact cratering processes, because (except for rare target cases, e.g., water ice [*Stewart et al.*, 2001]) crater excavation mechanisms do not predict near-vertical ejection according to the point source scaling model for crater excavation [e.g., *Houson and Holsapple*, 2011]. The self-secondary hypothesis is also questioning the robustness of age determination techniques using crater statistics [*Plescia and Robinson*, 2015], because the prevalent lunar crater production and chronology functions (and also those for Mercury and Mars) are largely based on crater counts on the continuous ejecta deposits of several Copernican-aged craters [e.g., *Neukum*, 1983]. However, the existence, abundance, significance, and formation mechanism of self-secondaries had not attracted much attention until the present generation of high-resolution images obtained by the Lunar Reconnaissance Orbiter Camera (LROC) [*Robinson et al.,* 2010] recently became available.

Using LROC images, crater density variations across different impact materials have now been recognized at several Copernican-aged craters on the Moon, e.g., Giordano Bruno [e.g., *Plescia*, 2010], Tycho [e.g., *Xiao and Strom*, 2012], and Aristarchus [e.g., *Zanetti et al.,* 2015]. The density difference is most obvious between ballistically emplaced ejecta deposits and melt ponds that are accumulated on top [e.g., *Xiao and Werner,* 2015]. However, complicated topography close to crater rims [*Morota et al.*, 2009], different degrees of rim collapse [*Boyce and Mouginis-Mark*, 2015], local resurfacing caused by the emplacement of impact melt [e.g., *Osinski et al.*, 2011], and potential effects of target properties on crater size-frequency distribution (SFD) [e.g., *Schultz and Spencer*, 1979] are all possible reasons for the observed crater density variations.

Clear evidence of some small craters on ballistically emplaced ejecta deposits being embayed by subsequent melt flows [e.g., *Zanetti et al.,* 2015] suggests the existence of self-secondaries. However, whether self-secondaries dominate the crater population on the continuous ejecta deposits requires an unambiguous identification of the self-secondary population. The different crater densities between ballistically emplaced ejecta deposits and melt ponds might indicate that self-secondaries dominate the small crater population on

the ballistically emplaced ejecta [e.g., *Xiao and Strom,* 2012; *Zanetti et al.,* 2015]. Alternatively, different target properties might also affect both the crater density and SFD on coeval surfaces as inferred from empirical scaling laws [e.g., *Schultz and Spencer,* 1979], although the extent of the effect is still controversial [e.g., *Zanetti et al.,* 2015]. Furthermore, many critical target property parameters for real lunar materials are lacking, which limits the application of cratering scaling laws [e.g., *Holsapple*, 1993].

While high-resolution numerical modeling continues to reveal the effect of different target properties on crater SFD [*Prieur et al.*, 2016], here we report an unambiguous identification of the self-secondary population on the continuous ejecta deposits of the Hokusai crater on Mercury (section 3). The emplacement history and formation mechanism of the self-secondaries are studied (section 4.1). The existence of such crater populations on other planetary bodies is discussed, together with their effect on the age determination technique using crater statistics (section 4.2).

2. Method and Data

The continuous ejecta deposits and floors of extremely young craters are the best locations to identify possible self-secondary populations, since these surfaces are little affected by subsequent impacts. Thanks to the high-resolution LROC data, however, lunar craters as young as South Ray (~2 Ma) [*Stöffler and Ryder*, 2001], Giordano Bruno (~4 Ma) [*Morota et al.,* 2009], and Tycho (~108 Ma) [*Stöffler and Ryder,* 2001] are shown to have accumulated abundant craters on the continuous ejecta deposits and crater floors [e.g., *Xiao and Strom,* 2012; *Hiesinger et al.,* 2012; *Zanetti et al.,* 2015]. Distinguishing self-secondaries from subsequently accumulated crater populations (i.e., primaries and/or distant secondaries) is another major controversy in planetary science [e.g., *McEwen and Bierhaus,* 2006; *Werner et al.,* 2009], hampered by recent debates about the effect of target properties on crater SFD. Therefore, there is no consensus on any confirmed self-secondary population on the Moon.

Mercury has more rayed craters (i.e., craters with optical ray systems) larger than 10 km diameter than the Moon [*Braden and Robinson*, 2013], and the rayed crater population on Mercury is younger than that on the Moon due to the larger surface erosion rate on Mercury [*Xiao et al.*, 2012]. The MErcury Surface, Space ENviroment, GEochemistry, and Ranging spacecraft (MESSENGER) [*Solomon et al.,* 2001] has successfully accomplished the over 4 year orbital operation about Mercury. Besides the multisets of high-resolution and multiband global mosaics, the highly elliptical orbit of MESSENGER has enabled the Mercury Dual Imaging System (MDIS) [*Hawkins et al.,* 2007] to obtain unprecedentedly high-resolution images for the northern hemisphere of Mercury ($>$10,000 frames are better than 5 m/pixel).

The Hokusai crater (diameter $D = 96$ km; 57.8°N, 16.8°E) on the northern hemisphere of Mercury is an ideal case to study whether self-secondaries dominate crater populations on the continuous ejecta deposits. It has the most pronounced ray system on the planet (Figure 1a), and the asymmetric pattern of the rays suggests that the impactor that formed Hokusai came from northeast to southwest. The circular rim and full development of continuous ejecta deposits around the crater rim (Figure 1b) suggest that the impactor trajectory had an inclination angle between 20 and 45° regarding the tangent plane [*Gault and Wedekind*, 1978]. The proto-peak ring on the crater floor and the quasi-layered ejecta (Figure 1b) are also unique among craters of its size [*Xiao and Komatsu*, 2013], suggesting that more impact melt may have been produced by Hokusai than similar-sized craters on Mercury, which was possibly caused by the larger than average impact velocity [*Xiao et al.*, 2014a, 2014b].

MDIS images with high resolution ($\leq$20 m/pixel) and large-incidence angles ($>$60°) cover more than 70% of the surface from ~3 crater radii to the center of Hokusai. Using the high-resolution MDIS images, the morphology and overlapping relationship of different crater materials of Hokusai are studied to reveal their emplacement sequences (section 3.1). Craters less than 100 m in diameter are clearly visible on the continuous ejecta deposits (Figure 1c). The different crater densities at various crater materials confirm the self-secondaries population of Hokusai (section 3.2).

3. Results

3.1. Different Crater Materials of Hokusai

Within the outer rim of the continuous ejecta deposits, the crater material of Hokusai can be classified into three facies according to their morphology and origin: ballistic ejecta deposits (e.g., Figure 1c), flow materials

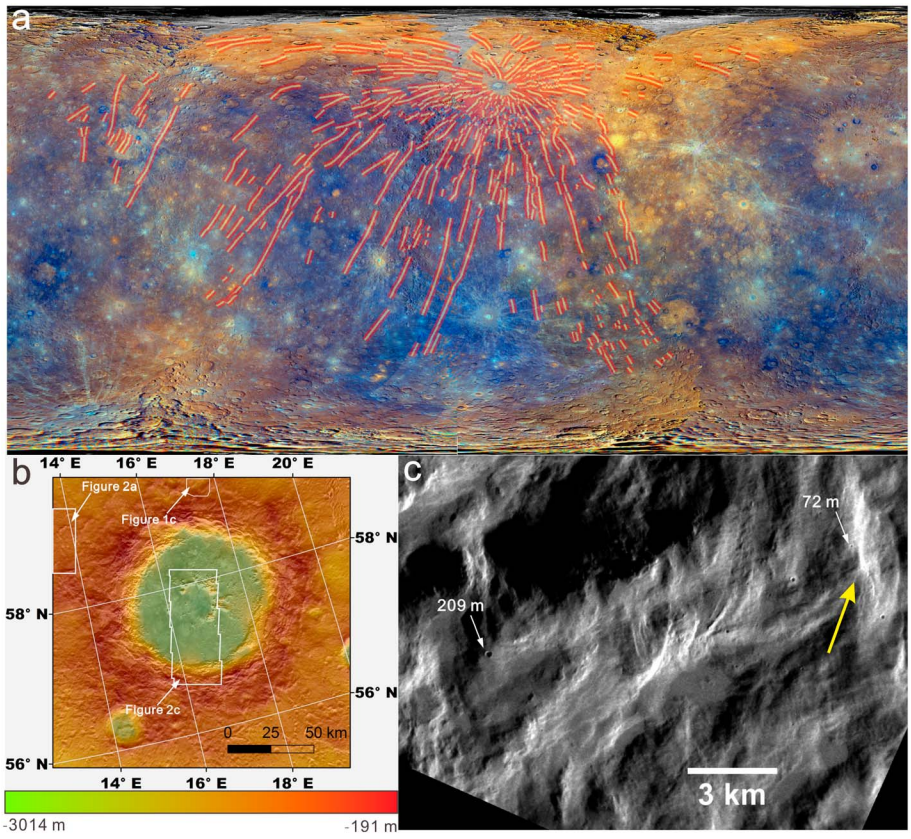

Figure 1. The Hokusai crater on Mercury and small craters on the continuous ejecta deposits. (a) The asymmetric ray system of Hokusai covers a large portion of the planet. The base mosaic is an enhanced color mosaic of Mercury (3.74 km/pixel; simple cylindrical projection centered on 0°N, 0°E). The red, green, and blue channels are the second principle component, the first principle component, and the ratio of the 430 nm/1000 nm filters, respectively, of the MDIS 8-band global mosaics. (b) Digital elevation model overlying monochrome mosaic shows the quasi-layered ejecta deposits around the crater rim. The map has a stereographic projection, which is centered on 57.76°N, 0°E. (c) High-resolution MDIS image (EN1015020937M; sinusoidal projection; 17 m/pixel; location is shown in Figure 1b) shows small craters on the continuous ejecta deposits of Hokusai (white arrows). The rough topography of this area (yellow arrow) is consistent with being ballistic ejecta deposits. Both the mosaics and digital elevation model are available at http://messenger.jhuapl.edu/the_mission/mosaics/.

(e.g., Figure 2a), and melt pools (e.g., Figure 2c). Continuous ejecta deposits are largely formed by ballistic ejecta with minor mixtures of local target material [*Schultz and Gault*, 1985], and they normally have rough surfaces. The ballistic ejecta deposits are not obvious around Hokusai because the subsequent flow materials have almost completely covered the rim circumferences (Figures 1b and 2a). In fact, the quasi-layered ejecta of Hokusai (e.g., Figure 2a) may be ballistic ejecta deposits that were displaced by the flow materials [*Xiao and Komatsu*, 2013]. The rough texture around the crater rim is consistent with the nature of ballistic ejecta deposits, and their existence is verified by occasionally exposed large blocks close to the crater rim (e.g., Figure 1c).

The flow materials exterior to the crater can extend continuously over 100 km from the crater rim (see Figure S1 in the supporting information). They have smooth textures at the ~20 m/pixel scale (Figure 2d). The thickness of the flow materials varies at different locations, but it is generally much less than 60 m, because craters ~1.2 km in diameter are only slightly filled by the flow materials (Figure 2a). Their occurrences are consistent with being impact melt (with certain amount of clasts) that was emplaced during the crater modification stage, and such melt flows are common around craters on other worlds [*Osinski et al.*, 2011]. The flows around Hokusai had much lower viscosity and larger speed than those on the Moon [*Denevi et al.*, 2012], because no flow channels, inflation budges, or longitudinal streamlines are visible along the flows. More importantly, the flows have swiped over local obstacles but did not fill shallow depressions (Figure 2a). They might have been emplaced in a mode comparable to ground hugging flows, although it is unlikely that volatiles had supported the flows [*Xiao and Komatsu*, 2013]. On the other hand, melt pools

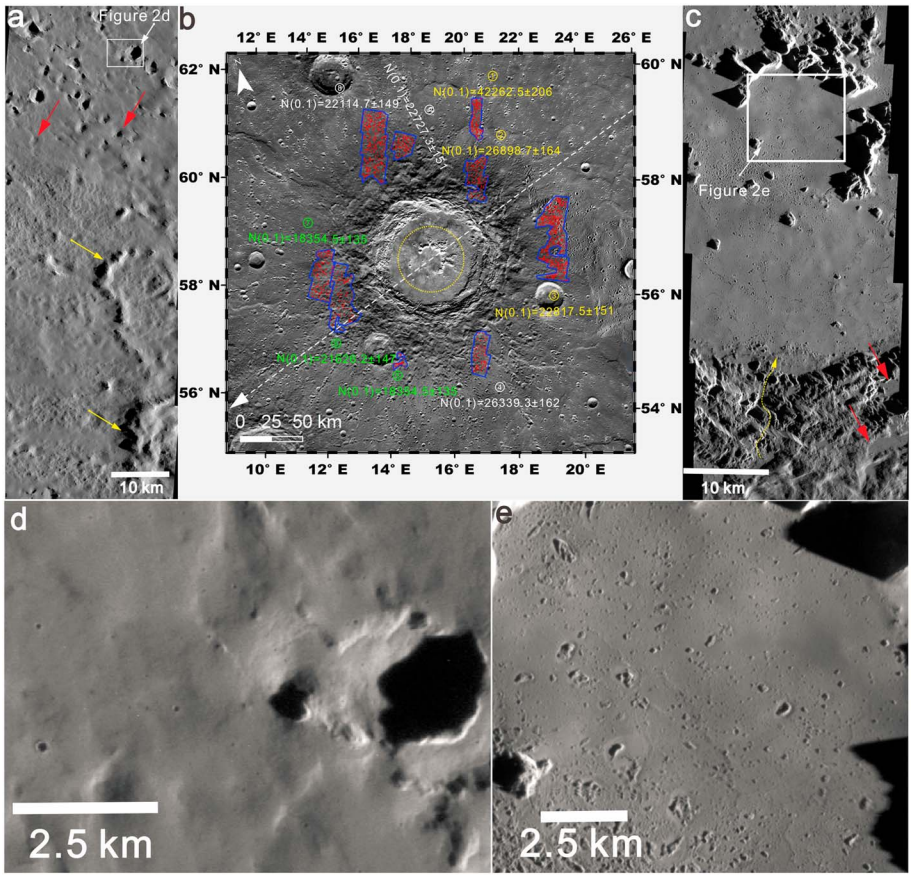

Figure 2. Different crater materials of Hokusai. (a) The northwestern part of the crater rim shows melt flows over both continuous ejecta deposits and secondary crater chains. The location of this image is marked in Figure 1b. Secondaries that are ~1–2 km in diameter (red arrows) are only slightly filled by the flow materials, indicating high flow speed. The yellow arrows point to the edges of the quasi-layered ejecta. (b) Crater densities on nine locations of melt flows around Hokusai (blue outlines). Craters are marked in red. $N(0.1)$ refers to the number of craters ≥0.1 km in diameter per million km^2 area, the errors are approximated by $N(0.1)^{1/2}$. The white arrow marks the approximate impact direction, and the yellow circle is the approximate location of the rim of the transient crater cavity (see Text S1 in the supporting information for the calculation). (c) Impact melt pools on the crater rim, terraces, and floor (red arrows). The yellow line follows a melt flow from the crater wall to the floor. (d) Many small craters postdated the melt flows are visible around Hokusai. The location of this area is marked in Figure 2a. (e) Few impact craters are visible on the melt pool on the crater floor. The location of this image is shown in Figure 2c. All the mosaics have stereographic projections centered on 57.76°N, 0°E, and north is toward the upper left of the panels. The lists of MDIS images used in making the mosaics and performing the crater counts are shown in the Table S1 of the supporting information.

are visible at local low-relief areas on the continuous ejecta deposits, crater terraces, and Hokusai's crater floor (Figure 2c). They were accumulated through melt flows from the surrounding higher relief areas, e.g., from crater wall to the crater floor. The whole crater floor is flat in general due to the infill of impact melt, and the uprange quarter of the floor is covered by a larger amount of collapsed materials (Figure 2b) [*Xiao et al.,* 2014b].

3.2. The Self-Secondary Crater Population of Hokusai

The melt flows are completely resurfaced units with respect to the preimpact surface. Therefore, the small craters on top of the melt flows clearly postdate the flows (Figure 2d), and they are either the self-secondary crater population created by Hokusai and/or crater populations younger than Hokusai. The small craters (D = ~30–400 m) on the nine different melt flows are collected. The datasets are completed for craters ≥0.1 km in diameter based on their clear appearances (i.e., >5 pixel dimensions of the base mosaics).

At least dozens of craters are collected at each area. However, mainly due to the small age of Hokusai, craters ≥0.1 km in diameter are not abundant enough for a reliable comparison of possible crater density differences on the nine areas using crater SFD (Figure S2a). Combining the nine crater populations, their SFD features a

steep differential slope of ~−4 (Figure S2b). The SFD is different from that of larger primary crater populations on Mercury, but it is consistent with that of typical secondary crater populations on planetary surfaces [e.g., *Strom et al.*, 2015]. However, whether the small primary crater population on Mercury similarly features steep SFD is not clear. Alternatively, the number of craters ≥0.1 km in diameter per 10^6 km^2, $N(0.1)$, is another expression of crater density if assuming random spatial distribution. The $N(0.1)$ densities for the nine counting areas are shown in Figure 2b, which vary by a maximum factor of ~2.5. Specifically, melt flows at the uprange of the crater rim have larger crater densities than those at the downrange (Figure 2b). Without effects from image resolution or topographic roughness of the counting areas, the different $N(0.1)$ densities cannot be caused by different degrees of resurfacing, because the craters collected clearly postdated the melt flows (e.g., Figure 2d). The larger crater density at the uprange is consistent with a recent observation that a simple lunar crater has an enhanced concentration of excavated boulders at the uprange [*Krishna and Senthil Kumar*, 2016]. The density variations, therefore, could suggest that the small crater populations are possibly dominated by self-secondaries of Hokusai.

Besides the above possible evidence, the most conclusive is the crater density difference between the flat crater floor and the melt flows. Under similar imaging conditions, craters are barely visible on the crater floor (e.g., Figure 2e), but they are much more abundant on both the melt flows (e.g., Figure 2d) and ballistic ejecta deposits (e.g., Figure 1c). Small primaries or distant secondaries from other craters that are younger than Hokusai should not have avoided appearing on the crater floor but being abundant all around the crater exterior. This contrast suggests that the observed small crater populations on the melt flows are not small primaries postdating Hokusai and/or distant secondaries formed by other craters, but they are dominated by the self-secondaries of Hokusai, which were emplaced before the crater floor had solidified to certain depths.

4. Discussion

4.1. Formation Mechanism of Self-Secondaries

During planetary impacts, materials are driven out of the final crater via four different mechanisms: (1) impact jetting during the initial contact stage launches superheated materials with both small ejection angles (<20°) and large velocities (may exceed ~2 times the impact velocity) [*Kieffer*, 1977; *Kurosawa et al.*, 2015], so they could eventually escape the gravity field of the target body [*Melosh*, 1989]; (2) spallation caused by the interaction of shock wave and rarefaction wave launches shallow target material from the interference zone, where rarefaction waves arrive earlier than the peak of shock waves [*Melosh*, 1984]; (3) initiated by shock waves and subsequently excited by rarefaction waves, the incompressible and subsonic excavation flows are the major mechanism of excavating materials, and most of the materials are deposited near the rim of the transient crater [*Melosh*, 1989]; and (4) the collapse of the excavation cavity (including the formation of central peaks/rings intertwined with the collapse) may push a small amount of impact melt and clasts toward the crater exterior [*Osinski et al.*, 2011].

The self-secondaries population of Hokusai is located on the melt flows, which cover the continuous ejecta deposits and some part of the secondaries chains, suggesting that the trajectory time of the fragments that formed the self-secondaries (t_{self}) is larger than that formed the continuous ejecta deposits and secondaries chains (t_{norm}). Excavation flows are not capable of forming the self-secondaries, because excavation flows have gradually decreasing velocities with larger launch distances from the impact site [*Houson and Holsapple*, 2011], and laboratory oblique impact experiments show that ejection angles during the excavation stage vary by less than ~15° (~35°–50°; [*Anderson et al.,* 2003]). Therefore, larger trajectory time in excavation flows generally means larger ejection velocity, thus longer ballistic ranges. The later arrival of self-secondaries on top of continuous ejecta deposits and secondary crater chains contradicts the hypothesis the fragments that formed the self-secondaries were launched by excavation flows.

The ballistic ranges of the fragments that formed the self-secondaries shown in Figure 2b are larger than ~22.5 km (i.e., distance from the transient crater rim to the final crater rim) and smaller than 135 km (i.e., distance from the crater center to the farthest self-secondaries collected). For these ballistic ranges, Figure 3a shows the possible combinations of ejection velocities and angles (from 35° to 85°) [*Polanskey and Ahrens*, 1990; *Anderson et al.,* 2003] using $l = v_e^2 \sin 2\theta / g$ (l the range, θ launch angle, v_e velocity, and surface gravity g), together with the corresponding trajectory time. t_{norm} can be regarded as a lower limit of t_{self}, meaning that

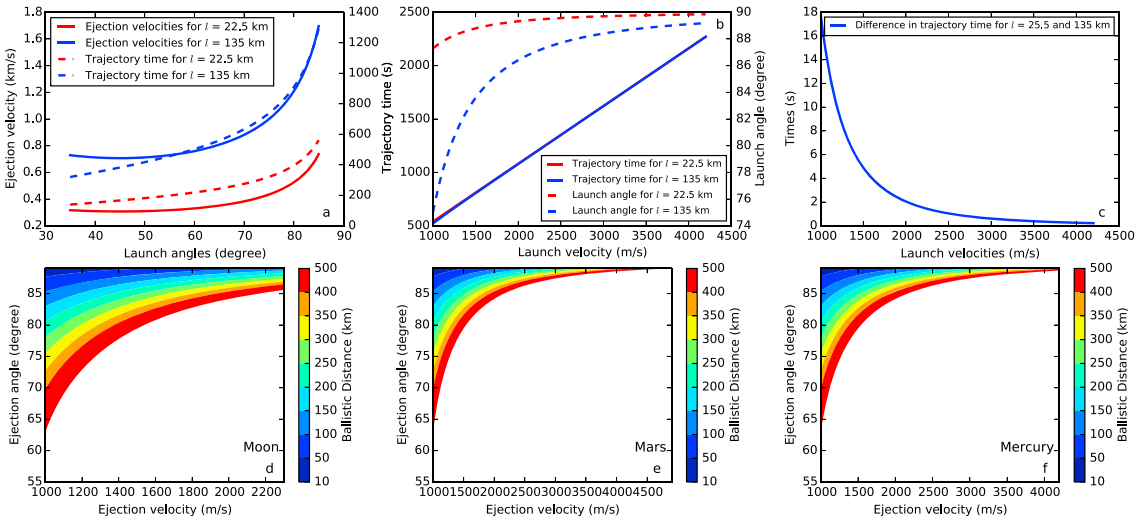

Figure 3. Ejection angles, velocities and travel time for different trajectory distances. (a) For ejection angles between 35 and 85°, the relationship between ejection velocities and trajectory time for ballistic ranges of 22.5 and 135 km. (b) For ejection velocities between 1 and 4.2 km/s, the relationship between ejection angles and trajectory time for ballistic ranges of 22.5 and 135 km. (c) Difference in trajectory time between same-velocity fragments that have ballistic ranges of 22.5 and 135 km. (d–f) For ejection velocities between 1 and 4.2 km/s and ejection angles between 55 and 89°, the possible ballistic ranges of self-secondaries on the Moon, Mercury, and Mars, respectively. The plots are cut off for ballistic distances larger than 500 km.

the self-secondaries were formed soon after the impact melt flowed over, which occurred immediately after the continuous ejecta deposits and secondary crater chains had been emplaced. This approximation might be akin to the formation of self-secondaries near the final crater rim. In this case, any fragment that has both larger ejection angles and velocities than those formed the continuous ejecta deposits and secondary crater chains are able to form the observed self-secondaries population (Figure 3a).

Another lower limit of t_{self} can be deduced from the minimum time the melt flows took to reach the locations where the self-secondaries are observed. Parameters such as viscosity or flow velocities of impact melt on Mercury are rarely studied. However, if most of the melt was pushed out of the transient crater by the formation of the structural uplift during the modification stage [*Osinski et al.*, 2011], a minimum velocity of ~90 m/s is estimated for the ~9 km structural uplift during the <100 s modification stage (see Text S2 for the calculation). If this velocity was coupled as an average velocity of the melt flows (i.e., comparable with fast ground hugging flows) [*Sparks et al.,* 1978], the flows took about 970 s from the final crater rim to a distance of 87 km. At this location, the fragments that formed the self-secondaries must have been launched before the modification stage was started, which had a duration >59 s (Text S1). Therefore, the minimum t_{self} for the fragments is about 1030 s. It indicates that the fragments that formed the self-secondaries should have ejection angles larger than 80° (Figure 3a), smaller flow velocities or longer crater modification stage would require larger t_{self}, and thus even larger ejection angles. For comparison, ballistic ejecta that formed the secondary crater chains had trajectory times of ~382 s if assuming ejection angles of ~45° (Figure 3a).

Impact spallation provides the launch mechanism for the fragments that formed the self-secondaries. Spallation starts earlier than the initiation of excavation flows, and spall fragments have much larger velocities (up to 80% of the impactor velocity) [*Polanskey and Ahrens*, 1990] than ejecta launched from the same position during the excavation stage [*Melosh*, 1984]. For craters that are larger than several kilometers in diameter on the Moon and Mars, spallation can launch target materials with velocities larger than the escape velocities, forming lunar and Martian meteoroids/meteorites [*Melosh*, 1984]. Indeed, most secondary crater chains and distant secondaries are formed by spallation [*Melosh*, 1989]. On the other hand, predictions based on shock mechanics [*Melosh,* 1984, Figure 6] and laboratory impact experiments [*Polanskey and Ahrens*, 1990] show that fragments are near-vertically launched during early spallation, but the evolution of launch angles during the entire course of impact spallation is little studied. Assuming the ejection velocities of fragments that formed the self-secondaries of Hokusai had an upper limit that equal the escape velocity of Mercury (4.26 km/s) and a lower limit of 1 km/s (i.e., corresponds to a trajectory time of 535 s for the ballistic range of 135 km; Figure 3a), the trajectory time and ejection angles for ballistic ranges of 25.5 km to 135 km

are shown in Figure 3b. Most, if not all, of these ejecta have large enough trajectory times to form the observed self-secondaries population, and their ejection angles and velocities are within the limit of those formed by impact spallation.

Fragments launched during early spallation have formed the late, melt superposing self-secondaries. This is consistent with the morphology of the self-secondaries, as they all have circular rims and scattered spatial distribution, and in agreement with near-vertical impact angles by single or highly clustered fragments [*Schultz and Gault*, 1985]. Shock mechanics predict that spalled fragments that are launched earlier have larger velocities but smaller sizes due to both the thinner interference zone and larger residual elastic energies [*Melosh*, 1985]. This echoes the observation that the self-secondaries are much smaller than those in secondary crater chains, which are likely formed by later-launched spall fragments. For fragments that have same launch velocities ($>$1 km/s) but different ejection angles, those landed ~135 km away only have slightly larger trajectory times ($<$20 s) than those landed ~25.5 km away (Figure 3c). This is consistent with the observation that secondaries are not observed on the melt pool on the crater floor, which has undergone longer adjustment and solidification [*Melosh and Ivanov*, 1999]. Alternatively, if spall fragments that have velocities less than 1 km/s can also form self-secondaries on the continuous ejecta deposits, especially those close to the crater rim (Figure 3a), some of them may have been erased by subsequent melt flows.

4.2. Effect of Self-Secondaries on Age Determination Using Crater Statistics

Vertically launched fragments via spallation should be inherent to impact cratering on all planetary bodies, because a shallow interference zone always exists due to the nonzero rise time of shock waves before reaching the peak pressure [*Melosh*, 1984]. Although the amount of such fragments varies at different bodies and impact sites [*Bart and Melosh*, 2010], self-secondaries should be visible around all craters on terrestrial planetary bodies, which have produced large enough spall fragments. As a general comparison, assuming that fragments forming self-secondaries on the Moon, Mercury, and Mars have velocities ranging from 1 km/s to their corresponding escape velocities, the possible occurrence ranges of self-secondaries around complex craters are computed (Figures 3d–3f). The first-order estimate shows that for a large range of crater diameters (i.e., scaled from the ballistic ranges) on the Moon, Mars, and Mercury, near-vertically launched fragments are theoretically capable to form self-secondaries on the continuous ejecta deposits and crater floors. Spallation may also form self-secondaries around craters on smaller bodies (such as 4Vesta and 1Ceres), although the morphology and spatial distribution of the self-secondaries might be different from those on both the Moon and terrestrial planets due to the smaller escape velocity and shorter rotation periods [*Neesemann et al.*, 2016].

Self-secondaries may affect the reliability of the age determination technique using crater count [*Plescia and Robinson*, 2015]. However, the extent of such effect may vary from case to case, such as different types and locations of crater materials and age of the parent crater. Fresh ballistic ejecta deposits, which have not been modified subsequently, should be dominated by self-secondaries. Crater materials that are emplaced later than most of the self-secondaries should be little affected, such as the melt pool on Hokusai's floor. However, the melt pools on the crater floor and rim of Tycho are much smaller and shallower than those on the crater floor of Hokusai [*Xiao et al.*, 2014b]. Recent morphological study suggested that the small crater population on top of them might also be dominated by self-secondaries, considering that their irregular morphology might be caused by low-velocity impacts [*Plescia*, 2015]. On the other hand, the accumulation of subsequent crater populations may gradually enlarge crater densities and hide the self-secondary crater population. For example, crater density differences between ballistic ejecta deposits and melt pools are visible at young craters such as Tycho and Giordano Bruno [*Xiao and Strom*, 2012], but it is not visible at older craters such as Copernicus [*Namiki and Honda*, 2003; *Hiesinger et al.*, 2012]. The accumulation of subsequent crater populations has caused equilibrium in the diameter range where self-secondaries occur [*Xiao and Werner*, 2015]. Therefore, the effect of self-secondaries on crater counts would be vanished for old enough craters.

5. Conclusions

As a confirmed self-secondary crater population, the Hokusai example reveals that spallation provides the launch mechanism for fragments forming self-secondaries on planetary bodies. For freshly formed complex craters on Mercury, the Moon, and Mars, self-secondaries should have formed on their crater floors and/or continuous ejecta deposits, and they should be visible if no subsequent modification has occurred

(e.g., resurfacing by impact melt or other cratering unrelated geological activity). Self-secondaries affect age determination of single young craters using crater counts on their ejecta deposits, but this effect is less obvious on crater materials that are emplaced long after the modification stage (e.g., large melt ponds). In addition, the accumulation of subsequent crater populations would exceed the self-secondaries population, so that self-secondaries would not be distinguishable around older craters. However, the critical age point beyond which self-secondaries do not affect crater count is not determined in this study. This is related to the absolute number of self-secondaries formed by impact craters versus the density of younger crater populations. Impact experiments and shock mechanics have predicted possible velocity size distributions of spall fragments [*Melosh*, 1984; *Polanskey and Ahrens*, 1990]. However, planetary impacts have more complicated fragmentations due to effects such as widespread heterogeneities in the target [*Melosh*, 1984]. Moreover, the observable self-secondaries may only represent a part of the whole self-secondaries population due to partial removal by subsequent modification. Therefore, a systematic study of the SFD evolution of small crater populations around different-aged craters may shade more light on this critical age point (e.g., Tycho and Copernicus) [*Xiao and Werner,* 2015].

Acknowledgments

All the data reported in this paper can be accessed by requesting to the corresponding author. This study is supported by the National Natural Science Foundation of China (41403053) and the fund CUG130106 of China University of Geosciences (Wuhan). Part of the data in this paper was collected during the support of the Research Council of Norway (235058/F20 CRATER CLOCK) and through the Centre of Excellence funding scheme, project 223272 (CEED). We thank the two anonymous reviewers for their helpful comments. The author declares no competing financial interests.

References

Anderson, J. L. B., P. H. Schultz, and J. T. Heineck (2003), Asymmetry of ejecta flow during oblique impacts using three dimensional particle image velocimetry, *J. Geophys. Res.*, *108*(E8), 5094, doi:10.1029/2003JE002075.

Bart, G. D., and H. J. Melosh (2010), Impact into lunar regolith inhibits high-velocity ejection of large blocks, *J. Geophys. Res.*, *115*, E08004, doi:10.1029/2009JE003441.

Boyce, J. M., and P. J. Mouginis-Mark (2015), Anomalous areas of high crater density on the rim of the Martian crater Tooting, *Workshop on Issues in Crater Studies and the Dating of Planetary Surfaces*, Abstract 9005.

Braden, S. E., and M. S. Robinson (2013), Relative rates of optical maturation of regolith on Mercury and the Moon, *J. Geophys. Res. Planets*, *118*, 1903–1914, doi:10.1002/jgre.20143.

Crater Analysis Techniques Working Group (1979), Standard techniques for presentation and analysis of crater size-frequency data, *Icarus*, *37*, 467–474, doi:10.1016/0019-1035(79)90009-5.

Croft, S. K. (1985), The scaling of complex craters: Proc. 15th Lunar Planet. Sci. Conf., *J. Geophys. Res.*, *90*, C828–C842.

Denevi, B. W., et al. (2012), Physical constraints on impact melt properties from Lunar Reconnaissance Orbiter Camera images, *Icarus*, *219*, 665–675, doi:10.1016/j.icarus.2012.03.020.

Gault, D. E., and J. A. Wedekind (1978), Experimental studies of oblique impact, *Proc. Lunar Planet. Sci. Conf.*, *9*, 3843–3875.

Grieve, R. A. F., P. B. Robertson, and M. R. Dence (1981), Constraints on the formation of ring impact structures based on terrestrial data, in *Multi-Ring Basins: Formation and Evolution*, *Proc. 15th Lunar Planet. Sci. Conf. 12A*, vol. 37–57, edited by P. H. Schultz and R. B. Merrill, pp. 37–57, Pergamon, New York.

Hawkins, S. E., II, et al. (2007), The Mercury Dual Imaging System on the MESSENGER spacecraft, *Space Sci. Rev.*, *131*, 247–338, doi:10.1007/s11214-007-9266-3.

Hiesinger, H., C. H. van der Bogert, J. H. Pasckert, L. Funcke, L. Giacomini, L. R. Ostrach, and M. S. Robinson (2012), How old are young lunar craters?, *J. Geophys. Res.*, *117*, E00H10, doi:10.1029/2011JE003935.

Holsapple, K. A. (1993), The scaling of impact processes in planetary systems, *Annu. Rev. Earth Planet. Sci.*, *21*, 333–373, doi:10.1146/annurev.ea.21.050193.002001.

Houson, K. R., and K. A. Holsapple (2011), Ejecta from impact craters, *Icarus*, *211*, 856–875, doi:10.1016/j.icarus.2010.09.017.

Kieffer, S. W. (1977), Impact conditions required for formation of melt by jetting in silicates, in *Impact and Explosion Cratering*, edited by D. J. Roddy, R. O. Pepin, and R. B. Merrill, pp. 751–769, Pergamon Press, New York.

Kneissl, T., S. van Gasselt, and G. Neukum (2011), Map-projection-independent crater size–frequency determination in GIS environments—New software tool for ArcGIS, *Planet. Space Sci.*, *59*(11–12), 1243–1254, doi:10.1016/j.pss.2010.03.015.

Krishna, N., and P. Senthil Kumar (2016), Impact spallation processes on the Moon: A case study from the size and shape analysis of ejecta boulders and secondary craters of Censorinus crater, *Icarus*, *264*, 274–299, doi:10.1016/j.icarus.2015.09.033.

Kurosawa, K., Y. Nagaoka, H. Senshu, K. Wada, S. Hasegawa, S. Sugita, and T. Matsui (2015), Dynamics of hypervelocity jetting during oblique impacts of spherical projectiles investigated via ultrafast imaging, *J. Geophys. Res. Planets*, *120*, 1237–1251, doi:10.1002/2014JE004730.

McEwen, A. S., and E. B. Bierhaus (2006), The importance of secondary cratering to age constraints on planetary surface, *Annu. Rev. Earth Planet. Sci.*, *34*, 535–567, doi:10.1146/annurev.earth.34.031405.125018.

Melosh, H. J. (1984), Impact ejection, spallation, and the origin of meteorites, *Icarus*, *59*, 234–260.

Melosh, H. J. (1985), Ejection of rock fragments from planetary bodies, *Geology*, *13*, 144–148.

Melosh, H. J. (1989), *Impact Cratering: A Geologic Process*, pp. 1–255, Oxford Univ. Press, New York.

Melosh, H. J., and B. A. Ivanov (1999), Impact crater collapse, *Annu. Rev. Earth Planet. Sci.*, *27*, 385–415.

Morota, T., et al. (2009), Formation age of the lunar crater Giordano Bruno, *Meteorit. Planet. Sci.*, *44*, 1115–1120.

Namiki, N., and C. Honda (2003), Testing hypotheses for the origin of steep slope of lunar size-frequency distribution for small craters, *Earth Planets Space*, *55*, 39–51.

Neesemann, A., T. Kneissl, N. Schmedemann, S. H. G. Walter, G. G. Michael, S. van Gasselt, H. Hiesinger, R. Jaumann, C. Raymond, and C. T. Russell (2016), Size-frequency distributions of km to sub-km sized impact craters on Ceres, *Lunar Planet. Sci.*, *47*, Abstract 2936.

Neukum, G. (1983), Meteoritenbombardement und Datierung planetarer Oberflachen, Habilitation thesis, Univ. of Munich, Germany.

Osinski, G. R., L. L. Tornabene, and R. A. Grieve (2011), Impact ejecta emplacement on terrestrial planets, *Earth Planet. Sci. Lett.*, *310*(3), 167–181, doi:10.1016/j.epsl.2011.08.012.

Pike, R. J. (1988), Geomorphology of impact craters on Mercury, in *Mercury*, edited by F. Vilas, C. R. Chapman, and M. S. Matthews, pp. 165–273, Univ. of Arizona Press, Tucson.

Plescia, J. B. (2010), Giordano Bruno: The young and the restless, *Lunar Planet. Sci.*, *41*, Abstract 2038.

Plescia, J. B. (2015), Lunar crater forms on melt sheets—Origins and implications for self-secondary cratering and chronology, *Lunar Planet. Sci*, *46*, Abstract 2054.
Plescia, J. B., and M. S. Robinson (2015), Lunar self-secondary cratering: Implications for cratering and chronology, *Lunar Planet. Sci*, *46*, Abstract 2535.
Polanskey, C. A., and T. J. Ahrens (1990), Impact spallation experiments: Fracture patterns and spall velocities, *Icarus*, *87*, 140–155.
Prieur, N. C., Z. Xiao, K. Wünnemann, and S. C. Werner (2016), Effects of target properties on crater sizes and its implications on age determination—Insights from numerical experiments, *Lunar Planet. Sci. 47*, Abstract 1988.
Robinson, M. S., et al. (2010), Lunar Reconnaissance Orbiter Camera (LROC) instrument overview, *Space Sci. Rev.*, *150*, 81–124, doi:10.1007/s11214-010-9634-2.
Schultz, P. H., and D. E. Gault (1985), Clustered impacts: Experiments and implications, *J. Geophys. Res.*, *90*, 3701–3732, doi:10.1029/JB090iB05p03701.
Schultz, P. H., and J. Spencer (1979), Effects of substrate strength on crater statistics: Implications for surface ages and gravity scaling, *Lunar Planet. Sci.*, *5*, 1081–1083.
Shoemaker, E. M., R. M. Batson, H. E. Holt, E. C. Morris, J. J. Rennilson, and E. A. Whitaker (1969), Observations of the lunar regolith and the Earth from the television camera on Surveyor 7, *J. Geophys. Res.*, *74*, 6081–6119, doi:10.1029/JB074i025p06081.
Solomon, S. C., et al. (2001), The MESSENGER mission to Mercury: Scientific objectives and implementation, *Planet. Space Sci.*, *49*, 1445–1465.
Sparks, R. S. J., L. Wilson, and G. Hulme (1978), Theoretical modeling of the generation, movement, and emplacement of pyroclastic flows by column collapse, *J. Geophys. Res.*, *83*, 1727–1739, doi:10.1029/JB083iB04p01727.
Stewart, S. T., J. D. O'Keefe, and T. J. Ahrens (2001), The relationship between rampart crater morphologies and the amount of subsurface ice, *Lunar Planet. Sci. Conf. XXXII*, Abstract 2092.
Stöffler, D., and G. Ryder (2001), Stratigraphy and isotope ages of lunar geologic units: Chronological standard for the inner solar system, *Space Sci. Rev.*, *96*, 9–54, doi:10.1023/A:1011937020193.
Strom, R. G., R. Malhotra, Z. Xiao, T. Ito, F. Yoshida, and L. R. Ostrach (2015), The inner solar system cratering record and the evolution of impactor populations, *Res. Astron. Astrophys.*, *15*(3), 407–434.
Werner, S. C., B. A. Ivanov, and G. Neukum (2009), Theoretical analysis of secondary cratering on Mars and an image-based study on the Cerberus plains, *Icarus*, *200*(2), 406–417, doi:10.1016/j.icarus.2008.10.011.
Xiao, Z., and G. Komatsu (2013), Impact craters with ejecta flows and central pits on Mercury, *Planet. Space Sci.*, *82*, 62–78.
Xiao, Z., and R. G. Strom (2012), Problems determining relative and absolute ages using the small crater population, *Icarus*, *220*, 254–267, doi:10.1016/j.icarus.2012.05.012.
Xiao, Z., and S. C. Werner (2015), Size-frequency distribution of crater populations in equilibrium on the Moon, *J. Geophys. Res. Planets*, *120*, 2277–2292, doi:10.1002/2015JE004860.
Xiao, Z., et al. (2012), The youngest geologic terrains on Mercury, *Lunar Planet. Sci.*, *43*, Abstract 2143.
Xiao, Z., R. G. Strom, C. R. Chapman, J. W. Head, C. Klimczak, L. R. Ostrach, J. Helbert, and P. D'Incecco (2014a), Comparisons of fresh complex impact craters on Mercury and the Moon: Implications for controlling factors in impact excavation processes, *Icarus*, *228*, 260–275, doi:10.1016/j.icarus.2013.10.002.
Xiao, Z., Z. Zeng, Z. Li, D. M. Blair, and L. Xiao (2014b), Cooling fractures in impact melt deposits on the Moon and Mercury: Implications for cooling solely by thermal radiation, *J. Geophys. Res. Planets*, *119*, 1496–1515, doi:10.1002/2013JE004560.
Zanetti, M., A. Stadermann, B. Jolliff, C. H. van der Bogert, H. Hiesinger, and J. B. Plescia (2015), Auto-secondary cratering vs target property effects on ejecta blankets of Copernican craters: What are the implications for age dating using small-diameter crater statistics?, *Lunar Planet. Sci.*, *46*, Abstract 1209.